Journal of Molecular Structure 1244 (2021) 131267

Contents lists available at ScienceDirect

Journal of Molecular Structure

journal homepage: www.elsevier.com/locate/molstr

Synthesis, characterization, surface analysis, optical activity and solvent effects on the electronic absorptions of Schiff base-functionalized amino thiophene derivatives: Experimental and TD-DFT investigations

Kifah S.M. Salih

Department of Chemistry and Earth Sciences, College of Arts and Sciences, Qatar University, P.O. Box 2713, Doha, Qatar

ARTICLE INFO

Article history:
Received 7 June 2021
Revised 28 July 2021
Accepted 7 August 2021
Available online 8 August 2021

Keywords:
Schiff base
Thiophene
Bathochromic shift
Tauc plot
TD-DFT

ABSTRACT

New derivatives of 3,3′-di-(((*E*)-(5-substituted-thiophen-2-yl)methylene)amino)-*N*-methylpropylamines (**3a,b**) were synthesized from the dehydration of *N*-methyl-diaminopropylamine and 2-thielylcarboxaldehyde derivatives; spectroscopically characterized by ^{1}H- and ^{13}C-NMR, IR, LC-MS, UV-Vis and elemental analysis. The nature of the electronic transitions of the SB compounds was investigated using Time-Dependent Density-Functional Theory (TD-DFT). Surface analysis and influence of solvent polarity on spectral properties were examined and established consequently. The molecular electrostatic potential (MEP) revealed that the two geometrical structures were found to be quite similar in term of electronic distributions. The presence of different electrophilic and nucleophilic sites located on the surfaces was suggested to stabilize the structures via classical H-bond and non-classical C-H…π interactions, in addition to interact with assorted solvent molecules. On the other hand, the solvatochromism of compound **3b** revealed a gradual shift to the red region through the increase of the solvent polarity, recording a 12 nm of bathochromic shift. The solvation relationship between the experimental λ_{max} and Gutmann's donicity numbers displayed a sense of positive linear behavior with a fluctuation, which was ascribed to a week interaction between molecules of solute and selected solvent. The band gap energy of compound **3a** was evaluated experimentally and computationally. Using optical absorption spectra, a value of – 3.801 eV was estimated following Tauc approach, while – 3.720 eV was resulting from TD-DFT simulation.

1. Introduction

The Schiff base (SB) functionalized compounds are substantial targets and have been receiving significant attention for possessing a wide applications in fields of chemistry and biology. The SB unit ($R^1R^2C{=}NR^3$) with the sp^2-hybridized carbon and nitrogen is well-known as imine or azomethine group in the chemical literature and exists in various natural and synthesized compounds. For instance, they are utilized as intermediate substrates in synthetic chemistry, polymer stabilizers and as dyes and pigments; they have furthermore been evaluated to display a potent biological activities, including antibacterial, antiviral, antiinflammatory, antiproliferative, antifungal, antimalarial, and antipyretic properties [1-3]. Derivatives of SBs are considered as a key point in advancing coordination chemistry. The coordination capability of the transition metal within the SB functional group allows the SB-containing compounds to turn as sensors; hence, playing a particular role in the growth of optical materials and inorganic biochemistry [4]. Fig. 1 exemplifies selected SB functionalized compounds with significant applications.

A tremendous number of synthetic protocols was established to synthesize a broad spectrum of SB compounds with diverse steric and electronic properties based on the classical condensation of aldehydes and ketones with primary amine derivatives in different solvents and conditions, though the involvement of dehydrating agents was frequently described [3]. In principle, stirring at room temperature for few hours is quite enough for reaction completion with aldehydes. However, ketones are in need of reflux condition for few hours to reach to end of reaction.

These fascinating compounds could involve in the formation of conventional hydrogen bond via the nitrogen atom with active moieties possessing NH, OH groups, giving rise to more stable

E-mail address: ksalih@qu.edu.qa

https://doi.org/10.1016/j.molstruc.2021.131267

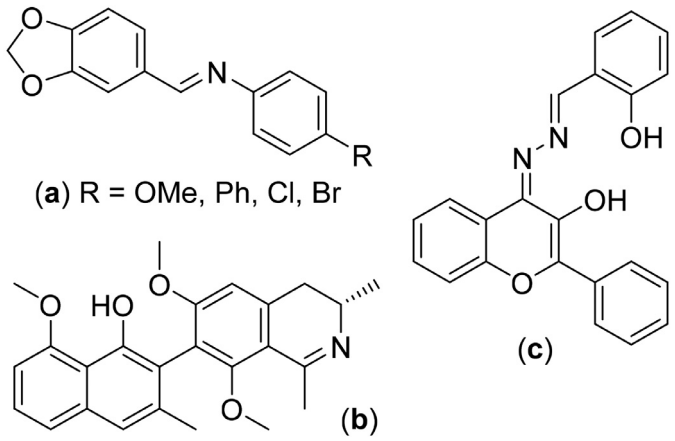

Fig. 1. Antifungal piperonal-SB compounds (a), Ancistrocladidine, a secondary metabolite produced by plants; an antimalarial agent (b) and a ratiometric fluorescent chemosensor for Al^{3+} (c).

structure. Additionally, noncovalent interactions are significantly involved in electronic perturbation within the molecular bonded systems. Although these interactions are weaker in contrast with their covalent counterparts, they are quite essential to give high molecular stability in liquid and solid states [5-7].

The solvatochromism is described as a reversible process of the absorption spectrum of a compound induced by the solvent molecules. The electronic system of such compound is subjected to perturbation, due to the interaction with the solvent [8]. Both molecular orbitals of the interacted species will be involved in the electronic transition, leading to a shift in the value of the λ_{max}. Subsequently, the solvation energy differences between the initial and excited state in various solvents point towards color change of that solution. The excited state is quite stable in more polar solvents than the initial state, leading to a bathochromic shift of the absorption maximum (positive solvatochromism). Whereas, less polar solvents influence the stability of the excited state than the initial state, demonstrating a counter-effect and resulting a hypsochromic shift of the λ_{max} (negative solvatochromism) [9, 10].

Based on the significant implementations of SB-functionalized compounds in the field of coordination chemistry and sensor applications, we were driven to synthesize new derivatives bearing a number of donor groups on almost a linear skeleton, which in turn could function as a multidentate ligand for upcoming investigation in catalysis [11]. Herein, we describe the synthesis of new 3,3′-di-(((*E*)-(5-substituted-thiophen-2-yl)methylene)amino)-*N*-methylpropylamines, resulting from condensation of *N*-methyldiaminopropylamine and 2-thielylcarboxaldehyde derivatives. The target compounds were fully identified by ^{1}H- and ^{13}C-NMR, IR, LC-MS, UV-Vis and elemental analysis. Surface analysis, influence of solvent polarity on spectral properties and optical activity were examined and established consequently; supported by DFT and TD-DFT calculations.

2. Experimental

2.1. Materials and measurements

All fine chemicals were of reagent quality and employed directly without any purification. 3,3′-Diamino-*N*-methyldipropylamine, 5-bromo-2-thiophenecarboxaldehyde, 5-nitro-2-thiophenecarboxaldehyde and anhydrous sodium sulfate were procured from Sigma Aldrich. Bruker ALPHA FTIR spectrometer was put in use to perform all transmission spectra in solid state in the range of 400–4000 cm^{-1}. The CHN analysis was evaluated employing Thermo Scientific™ FLASH™ 2000 Organic Elemental Analyzer. JOEL 600 MHz spectrometer was utilize to record ^{1}H- and ^{13}C-NMR spectra with internal reference to the residual solvent signal, chloroform-d: δ = 7.26 ppm for ^{1}H-NMR and δ = 77.16 ppm for ^{13}C-NMR. The UV-Vis measurements were performed using Agilent 8453 single beam spectrophotometer; solvent of UV spectrophotometric grade were used, including ethanol, tetrahydrofuran, *N,N*-dimethylformamide, dimethyl sulfoxide, acetone, dichloromethane and acetonitrile. LC/MS analysis was accomplished on a 6460 Triple Quadrupole LC/MS Spectrometer.

2.2. Computation and visualization

In this work, the B3LYP functional [12, 13] was chosen as a method, since it includes considerable effects of electron correlation and has been widely used for decades by the scientific community. It turned to a trustworthy access to pursue the molecular geometry, electronic spectroscopy and conformational stability, in particular for simple and neutral molecules possessing atoms from the first and second rows of the periodic table [14-16]. The basis set is the second element of model chemistry, in which Pople basis sets were preferred to be employed along with double diffuse functions to perform accurate and less expensive calculations [17, 18]. Thus, all DFT calculations were achieved using Gaussian W09 Revision E.01 software [19]. Unless otherwise stated, the B3LYP functional method with 311G++(d,p) basis set were harnessed to perform the optimization of molecular geometry and calculation of frequencies for the new structures. The checkpoint file was used to map the molecular electrostatic potential (MEP) and to generate the molecular orbital energy levels via GaussView software. The spectrum of density of states (DOS) was plotted from the optimized or TD-DFT output file using GaussSum software through plotting energy versus partial density of states, orbitals with the FWHM = 0.2 [20].

2.3. Synthesis of 3,3′-di-(((E)-(5-bromothiophen-2-yl)methylene)amino)-N-methylpropylamine (3a)

The target compound was synthesized following conventional condensation reactions. A solution of 757 mg (5.0 mmol) of 3,3′-diamino-*N*-methyldipropylamine in 10 mL of THF was added portion-wise to a stirred solution of 2011 mg (10.0 mmol) of 5-bromo-2-thiophenecarboxaldehyde in 10 mL of THF in 50-milliliter round-bottomed flask. The mixture was stirred at room temperature for 3 h and then the volatile was removed under reduced pressure. The residue was purified by column chromatography using ethyl acetate and hexane as eluent solvent, yielding green-colored oily-like product in 77% (1.90 g). ^{1}H-NMR (600 MHz, $CDCl_3$): δ = 8.19 (t, J = 1.3 Hz, 2H, *HC*=N), 6.98 (d, J = 3.8 Hz, 2H, C*H*-thienyl), 6.97 (d, J = 3.9 Hz, 2H, C*H*-thienyl), 3.53 (td, J = 6.9, 1.3 Hz, 4H, CH_2NCH_3), 2.38 (t, J = 6.9, 4H, CH_2N=CH), 2.20 (s, 3H, NCH_3), 1.80 (quint, J = 6.9 Hz, 4H, $CH_2CH_2CH_2$) ppm. ^{13}C-NMR (151 MHz, $CDCl_3$): δ = 153.63 (s, 2C, HC=N), 144.22 (s, 2C, *C*-thienyl), 130.34 (s, 2C, *C*H-thienyl), 130.21 (s, 2C, *C*H-thienyl), 116.74 (s, 2C, *C*Br), 59.05 (s, 2C, CH_2NCH_3), 55.19 (s, 2C, CH_2N=CH), 42.17 (s, 1C, NCH_3), 28.26 (s, 2C, $CH_2CH_2CH_2$) ppm. LC-MS (ESI), *m/z*: 493.9 $[M]^+$, 491.9 $[M]^+$, 489.9 $[M]^+$, 318.0 $[M]^+$, 288.2 $[M]^+$, 244.2 $[M]^+$, 102.1 $[M]^+$ and 74.1 $[M]^+$. Selected IR frequencies (cm^{-1}): 3095 $\nu_{(C\text{-}Hthienylic)}$, 2910 $\nu_{(C\text{-}Haliphatic)}$, 1630 $\nu_{(C=N)}$, 1621 $\nu_{(C=C)}$ cm^{-1}. Anal. Calcd. for $C_{17}H_{21}Br_2N_3S_2$: C, 41.56; H, 4.31; N, 8.55. Found: C, 41.86; H, 4.22; N, 8.62. UV/Vis. Abs. in EtOH, λ_{max} = 203 and 292 nm.

2.4. Synthesis of 3,3′-di-(((E)-(5-nitrothiophen-2-yl)methylene)amino)-N-methylpropylamine (3b)

In a similar manner to the abovementioned synthesis, a solution of 757 mg (5.0 mmol) of 3,3′-diamino-*N*-methyldipropylamine in 10 mL of THF was added portion-wise to a stirred solution of 1604 mg (10.0 mmol) of 5-nitro-2-thiophenecarboxaldehyde in 10 mL of THF in 50-milliliter round-bottomed flask. The mixture was stirred at room temperature for 3 h and then the volatile was removed under reduced pressure. The residue was purified by column chromatography using ethyl acetate and hexane as eluent solvent, giving black-colored sticky solid product in 79% (1.67 g). ^{1}H-NMR (600 MHz, $CDCl_3$): δ = 8.31 (t, J = 1.3 Hz, 2H, *H*C=N), 7.82 (d, J = 4.2 Hz, 2H, C*H*-thienyl), 7.17 (d, J = 4.2 Hz, 2H, C*H*-thienyl), 3.64 (td, J = 6.8, 1.1 Hz, 4H, CH_2NCH_3), 2.49 (t, J = 6.8 Hz, 4H, CH_2N=CH), 2.28 (s, 3H, NCH_3), 1.87 (quint, J = 6.8 Hz, 4H, $CH_2CH_2CH_2$) ppm. ^{13}C-NMR (151 MHz, $CDCl_3$): δ = 153.50 (s, 2C, HC=N), 152.97 (s, 2C, CNO_2), 148.67 (s, 2C, *C*-thienyl), 128.56 (s, 2C, *C*H-thienyl), 128.06 (s, 2C, *C*H-thienyl), 58.96 (s, 2C, CH_2NCH_3), 55.00 (s, 2C, CH_2N=CH), 41.95 (s, 1C, NCH_3), 27.86 (s, 2C, $CH_2CH_2CH_2$) ppm. LC-MS (ESI), m/z: 331.1 $[M\text{-}2NO_2]^+$, 288.2 $[M]^+$, 244.2 $[M]^+$, 102.1 $[M]^+$ and 74.1 $[M]^+$. Selected FTIR frequencies (cm^{-1}): 3101 $\nu_{(C\text{-}Hthienylic)}$, 2938 $\nu_{(C\text{-}Haliphatic)}$, 1628 $\nu_{(C=N)}$, 1620 $\nu_{(C=C)}$, 1360 $\nu_{(N=O)}$ cm^{-1}. Anal. Calcd. for $C_{17}H_{21}N_5O_4S_2$: C, 48.21; H, 5.00; N, 16.54. Found: C, 47.98; H, 4.69; N, 16.46. UV/Vis. Abs. in EtOH, λ_{max} = 200 and 333 nm.

3. Results and discussion

3.1. Synthesis and characterization

The two new SB derivatives (**3a** and **3b**) were smoothly prepared from the dehydration reaction of *N*-methyldiaminopropylamine and 2-thielylcarboxaldehyde precursors in THF as a solvent at room temperature. High yields of oily and sticky products were obtained; the compounds were found to be soluble only in polar and less polar organic solvents such ethanol, DMSO, THF, acetone dichloromethane. Thorough characterization of the SB derivatives were performed spectroscopically, displaying the expected structures as shown in Scheme 1.

The ^{1}H-NMR spectroscopy in $CDCl_3$ revealed all resonances for the two structures in a very close range, Fig. S1-S2. In both compounds, three sets of multiple signal appeared at the range of 1.78-3.65 ppm were assigned for the symmetrical methylene groups, while the N-CH_3 peaks were appeared at 2.20 and 2.28 ppm. The two sets of multiplet splitting peaks of the thienyl CH were adjacent in **3a**, 6.96 and 6.99 ppm. Whereas, a wide separation was detected in **3b** for such protons, 7.17 and 7.82 ppm. The great chemical shift between these two protons is ascribed to the high electronic influence of the NO_2 group on the thienyl ring. As anticipated, the CH peaks of the imine functional group were observed as triplet resonance at 8.19 and 8.31 ppm. Moreover, the ^{13}C-NMR of both compounds exemplified all the corresponding aliphatic, thienylic and iminic carbon signals with the predicted range of chemical shifts in the spectra, Fig. S3-S4.

The FT-IR transmissions of starting materials and the SB compounds are presented in Fig. 2a,c. The disappearance of the two weak N–H stretching bands at 3360 and 3311 cm^{-1} of the triamine substrate indicated the formation of imine functional groups in the new products. The observed stretching bands in the range of 3074 to 2845 cm^{-1} were attributed to the characteristic thienylic and aliphatic C–H absorption frequencies. These bands were presented as well in the aldehyde starting materials and only the aliphatic frequencies in the triamine substrate. The spectra of **3a** and **3b** illustrated clearly strong band at 1630 and 1632 cm^{-1}, respectively

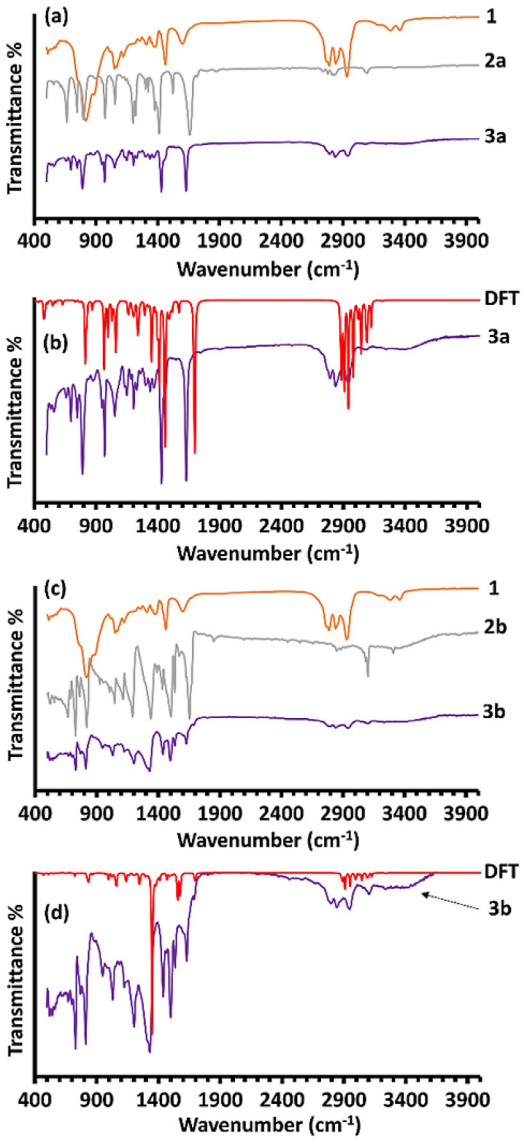

Fig. 2. FTIR of **3a** (a), DFT-IR of **3a** (b), FTIR of **3b** (c) and DFT-IR of **3b** (d).

for the vibration of C=N. Additional bands for other vibrational modes belongs to C–C, C=C, C–N and N=O were also observed in the recorded spectra [21]. Furthermore, the simulated DFT-IR of the new compounds displayed a sophisticated level of agreement with experimental results, as displayed in Fig. 2b,d.

The expected molecular formulas was further identified using CHN elemental analysis, in which a range of satisfactory figures was fitting with of the anticipated structures. The LC-MS (ESI) spectrum of **3a** reflected the expected three major mass-to-charge ratio (m/z) peaks (493.9 $[M]^+$, 491.9 $[M]^+$ and 489.9 $[M]^+$), as bromine has two naturally stable isotopes, ^{79}Br and ^{81}Br in approximately 1:1 ratio, Fig. S5. Likewise, a m/z of 331.1 $[M\text{-}2NO_2]^+$ was detected by **3b** due to the fragmentation of the two fragile NO_2 groups, Fig. S6 [22]. Notably, both **3a** and **3b** share similar fragments, such as 288.2 $[M]^+$, 244.2 $[M]^+$, 102.1 $[M]^+$ and 74.1 $[M]^+$.

3.2. Electronic absorptions and electronic transitions

The UV-Vis absorption spectra of starting materials and products were recorded in the spectral area of 190–800 nm in neat ethanol. Though the two compounds have an identical scaffold and vary only on the 5-position of thienyl moiety (5-bromo in **3a** and

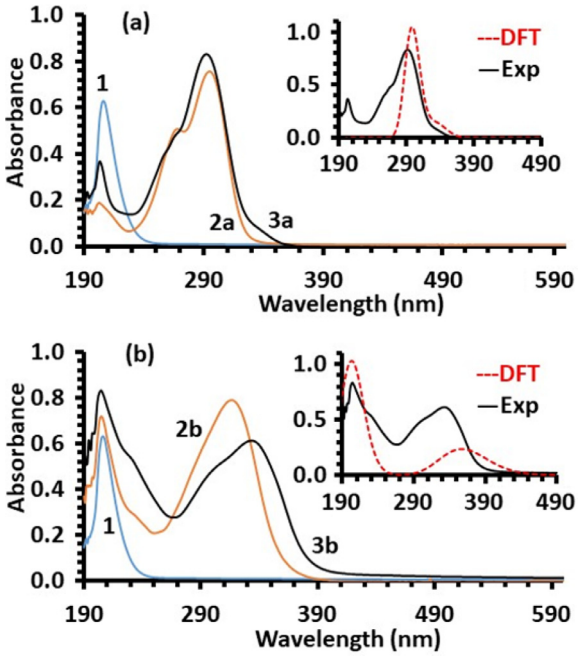

Fig. 3. UV-Vis of reactants and products, insets display the experimental and simulated spectra, of **3a** (a) and **3b** (b), the later was shifted by 155 nm toward blue region to fit with experimental [23].

5-nitro in **3b**), the overall features of the spectra of these compounds were not similar, because the electronic structure of the boundary orbitals is influenced by the substituents on the thienyl ring. The triamine precursor (**1**) displayed a maximum absorption in the UV area at 206 nm, resulting from n-σ^* electron transition, however, the carboxaldehyde **2a** mainly exhibited two absorption at λ_{max} = 203 and 295 nm; the later overwhelms a shoulder at 268 nm. The SB product (**3a**) resulting from these materials revealed also two broad bands with maximum absorptions at 203 and 292 nm, in which the shoulder was merged with main absorption due to hypsochromic effect (blue shift), Fig. 3a. These electronic transitions could be ascribed to n-σ^*, π-π^* and n-π^* transitions. The carboxaldehyde **2b** showed a maximum absorption at λ_{max} = 205, overwhelming a shoulder at 235 nm, and a major band at 316 nm. However, compound **3b** exhibited two intense electronic absorptions, a band with a λ_{max} = 200 nm having a shoulder at 230 nm and strong band at 333 nm (red shift) with a shoulder at about 300 nm. These absorptions were resonated again to n-σ^*, π-π^* and n-π^* transitions, Fig. 3b. The observed hypsochromic effect in **3a** and bathochromic effect in **3b** emphasize the formation of the SB-functionalized products through the condensation process.

To investigate the nature of the electronic transitions of the SB compounds, the excitation state were calculated at the TD-DFT level of theory using the optimized structures and the hybrid B3LYP functional with basis set of 6-311++G(d,p) in ethanol. Solvation model was accomplished employing the Polarizable Continuum Model (PCM) via the Integral Equation Formalism version (IEFPCM); this approach allows the generation of solute cavity through a series of overlapping spheres [24]. As seen in the insets of Fig. 3(a) and 3(b), an adequate agreement is observed between the experimental UV–Vis and simulated TD-DFT spectra. On the other hand, the main excited states resulting from the simulations permitted the interpretation of the experimental spectra; Table 1 displays all the electronic transitions along with their oscillator strengths and energies.

These transitions are in general very close to the experimental bands [25]. For instance, the intense experimental bands at 292 nm in **3a** corresponds mainly to H-2→L+1 and H-1→LUMO, in addition to two minor transitions at higher wavelength match the HOMO→L+1 and HOMO→LUMO with oscillator strength of 0.10 and 0.01, respectively. It is notable that the molecular orbitals in LUMO and L+1 are delocalized on the imine and the thienyl moieties and possessing almost the same shape of orbital distribution, due the minimal difference in their energy values, (-0.19849 au and -0.19821 au, respectively). The difference in energy applies as well to HOMO and H-1 orbitals, while H-2 displays obvious variance in reference to H-1 with majority of orbital lobes delocalized on the methylated N atom, Fig. S7.

Furthermore, the intense experimental bands at 200 nm in compound **3b** is resulting from H-4→L+1, H-3→LUMO, H-2→L+1 and H-1→LUMO with oscillator strength equals to 0.19. The second broad band at 333 nm corresponds to HOMO→LUMO and HOMO→L+1 transitions with oscillator strength 0.01 and 0.04, respectively. Again, it is obvious that the molecular orbitals are predominantly delocalized on the imine and the thienyl groups except in HOMO, where the lobes are delocalized on the methylated N atom. The HOMO also involves the localization of atomic orbitals belonging to the scaffold, Fig. S8.

3.3. Surface analysis and solvatochromism

To associate the stability and interaction with molecular electronic structure, the geometry of the two compounds was optimized to ground state in vacuum. The two geometrical structures were very similar in term of electronic distributions, taking into account that the only difference is located on the 5-position of thienyl moiety. As shown by the molecular electrostatic potential, the electrophilic and nucleophilic sites are located on the surface of the two structure, Fig. 4. The electronic density is reflected by the potential decrease, which ranges from red (high), orange, yellow, white to blue (low). Hence, the three N atoms in each molecule in addition to O atoms of the NO_2 groups in **3b** possess the highest nucleophilic sites (red color), while the electrophilic sites (white to blue) are greatly located on the S atoms and C of imine moieties. The rest of scaffold atoms is exemplified by yellow, illuminating moderate nucleophilic sites. These various sites are expected to stabilize the structure via classical (H-bond) and non-classical (C-H…π) interactions, in addition to interact with different solvent molecules [26-29].

The solvatochromism is commonly considered to evaluate the ground- and excited-states, study the effect of solvent on maximum absorption wavelength and to examine the conformation and binding of structures, [30]. The impact of diverse solvents on the absorption spectra of the new compounds was pursued to evaluate the solvatochromic effect. For solubility issue, the experiments were carried out using neat polar and less polar solvents, involving ethanol, dimethyl sulfoxide, dimethylformamide, ethyl acetate, acetonitrile, tetrahydrofuran and dichloromethane. In the one hand, a significant shift of the maximum absorption of **3a** was not detected in different solvent than ethanol, thus, this compound was ruled out from the detailed investigation. On the other hand, a remarkable transformation in the solvatochromism pattern for compound **3b** was established in the region of 280-420 nm, Fig. 5a. The maximum absorption in ethanol (λ_{max} = 333 nm) was gradually shifted to the red region through the increase of the polarity of the harnessed aprotic solvent, particularly with DMF and DMSO. The higher λ_{max} was observed with DMSO (345 nm), denoting to a 12 nm of bathochromic shift. This behavior could be rationalized to the fact that the excitation state of the type π-π^* is more stable in polar solvent, meanwhile, leading to low energy gap. In order to study the solvation relation between the observed λ_{max}

Table 1
Oscillator strengths and energies of all electronic transitions.

Comp.	λ (nm)	Osc. Strength	Major Contributions	ΔE (eV)
3a	334	0.10	HOMO->L+1 (99%)	3.7150
	333	0.01	HOMO->LUMO (99%)	3.7196
	297	0.91	H-2->L+1 (36%), H-1->LUMO (62%)	4.1688
3b	356	0.04	HOMO->L+1 (100%)	2.4246
	355	0.01	HOMO->LUMO (100%)	2.4304
	202	0.19	H-4->L+1 (34%), H-3->LUMO (34%), H-2->L+1 (10%), H-1->LUMO (17%)	3.4746

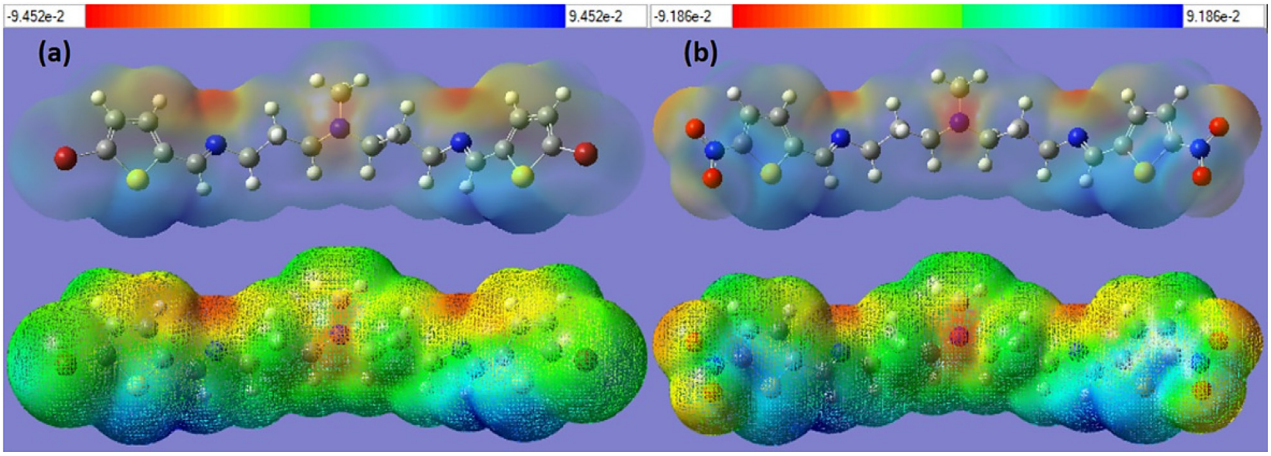

Fig. 4. Molecular electrostatic potential in transparent and mesh formats of **3a** (a) and **3b** (b).

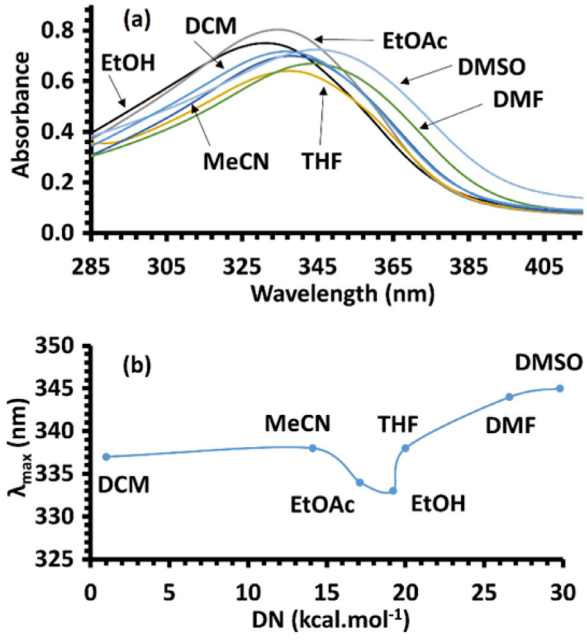

Fig. 5. Solvatochromism investigation of **3b** in different solvents (a) and solvation relation: λ_{max} vs Gutmann's solvent donor numbers (b).

and Gutmann's donicity numbers (DN) [31, 32], a sense of positive linear behavior was revealed with a fluctuation resulting from ethyl acetate and ethanol solvents, Fig. 5b. This discrepancy could be ascribed to the week interaction between solute and solvent molecules.

3.4. Optical bandgap estimation

The measurement of absorption-based spectra is commonly employed techniques to determine the optical bandgap for predicting photophysical and photochemical properties of materials to be used in optoelectronic devices. The bandgap energy (E_g) is defined by the required energy to excite an electron from the valence band (HOMO) to the conduction band (LUMO). An approach for evaluating the bandgap energy was described by Tauc in 1966 using optical absorption spectra [33]. The method involves the assumption that the energy-dependent absorption coefficient (α) can be indicated by the following equation: $(\alpha \cdot h\nu)^{1/\gamma} = B(h\nu - E_g)$, in which h is the Planck constant, ν is a frequency of a photon and B is a constant. The γ is based on the electron transition and is equal to ½ or 2 for material with direct or indirect allowed transition gaps, respectively [34, 35].

The value of α could be determined directly from Beer–Lambert's relation, $\alpha = 2.303A/d$, where A is the absorbance recorded from the UV–Visible measurement and d is the path length of the quartz cuvette in cm [36, 37]. Accordingly, the experimentally determined electronic absorptions (A and λ) of the selected compound (**3a**) was first converted to reflectance-absorption spectrum according to aforementioned equations. Upon plotting the $(\alpha \cdot h\nu)^{½}$ against the photon energy, the E_g is characterized by an area displaying a steep and linear increase of light absorption with increasing energy. As a result, extrapolating this linear region to the abscissa gives an estimate of the optical bandgap energy of compound **3a**, $E_g = -3.801$ eV (Fig. 6a), which is very close to the resulting value from TD-DFT simulation (– 3.720 eV, Table 1, entry 2).

Moreover, the spectrum of density of states (DOS) was plotted from the same TD-DFT output file using GaussSum software through plotting energy versus partial density of states, giving a

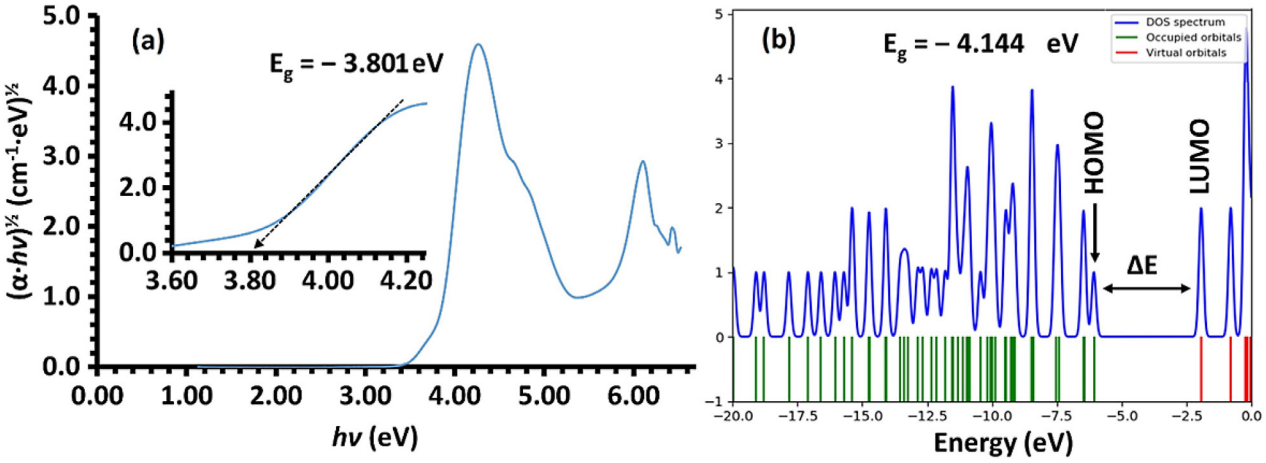

Fig. 6. Tauc plot derived from UV-Vis of **3a**, the inset displays the estimated optical gap (a); DOS spectrum of **3a**.

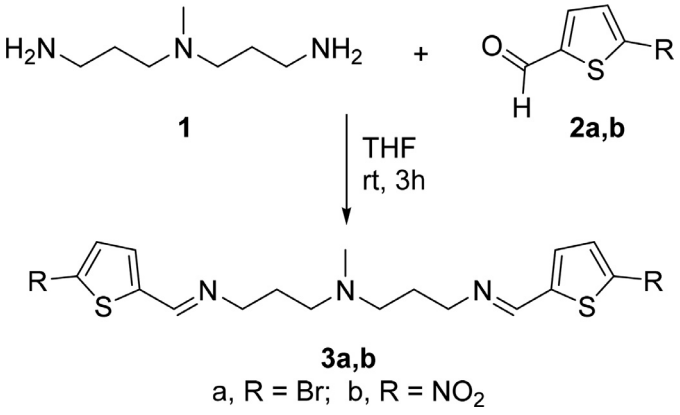

Scheme 1. Condensation of *N*-methyl-diaminopropylamine and 2-thielylcarboxaldehyde derivatives.

value equals to – 4.144 eV of energy gab, Fig. 6b. It is worth mentioning that the gap acquired from LUMO-HOMO or DOS is approximately a fundamental band gap [38]. In general, the optical gap is considerably lower than the fundamental one for the reason that in the excited state the electron and hole stay bound to one another electrostatically. Hence, the value of the electron–hole pair binding energy should be subtracted from – 4.144 eV to yield the optical bandgap [39].

Based on these outcomes, the two compounds could be used as nonlinear optical organic materials to produce a nonlinear response, since they demonstrated satisfactorily interaction with light. Additionally, their bandgap energies are laying within the range of wide-bandgap materials (2–4 eV). These materials possess in general electronic properties fall in between conventional semiconductors and insulators [40].

4. Conclusion

Derivatives of 3,3′-di-(((*E*)-(5-substituted-thiophen-2-yl)methylene)amino)-*N*-methylpropylamine were synthesized in very good yields from the dehydration reaction of *N*-methyl-diaminopropylamine and 2-thielylcarboxaldehydes. Spectroscopic techniques identified the proposed structures, which were further investigated by DFT calculations. The observed hypsochromic effect in **3a** and bathochromic effect in **3b** highlight the formation of the SB-functionalized products. The basis of the electronic transitions of the SB compounds was investigated using TD-DFT. Surface analysis was pursued through the molecular electrostatic potential (MEP), revealing that the two geometrical structures were found to be quite similar in term of electronic distributions. The presence of different electrophilic and nucleophilic sites located on the surfaces are expected to stabilize the structure via classical H-bond and non-classical C-H…π interactions, in addition to interact with various solvent molecules. Furthemore, the influence of solvent polarity on spectral properties were studied and established consequently via solvatochromism. Compound **3b** revealed a gradual shifting to the red region through the increase of the solvent polarity, recording a 12 nm of bathochromic shift. A sense of positive linear behavior was observed, when solvation relation was set between the experimental λ_{max} and Gutmann's donicity numbers. The bandgap energy of compound **3a** was evaluated experimentally and computationally. Using optical absorption spectra, a value of – 3.801 eV was estimated following Tauc approach, while – 3.720 eV was resulting from TD-DFT simulation. These results suggests that the new compounds could be employed as organic material for nonlinear activity, and as appropriate multi-dentate ligands through the three N atoms.

Credit Author Statement

Not applicable for single author.

Declaration of competing interest

The author declares that he has no conflicts of interest.

Acknowledgment

Open access funding provided by the Qatar National Library. The Qatar National Research Fund supported this research through NPRP11S-1204-170062. The author gratefully acknowledges the Central Laboratories Unit, Qatar University for accomplishing the analysis. Stimulating discussions with Dr. I. Warad and Dr. M. Shibl gratefully acknowledged. Computer time has been generously provided by the Information Technology Services at Qatar University.

Supplementary materials

Supplementary material associated with this article can be found, in the online version, at doi:10.1016/j.molstruc.2021.131267.

References

[1] G. Bringmann, M. Dreyer, J.H. Faber, P.W. Dalsgaard, J.W. Jaroszewski, H. Ndangalasi, F. Mbago, R. Brun, S.B. Christensen, Ancistrotanzanine C and Related 5,1'- and 7,3'-Coupled Naphthylisoquinoline Alkaloids from Ancistrocladus tanzaniensis, J. Nat. Prod. 67 (5) (2004) 743–748.

[2] P. Przybylski, A. Huczynski, K. Pyta, B. Brzezinski, F. Bartl, Biological Properties of schiff bases and Azo derivatives of phenols, Cur. Org. Chem. 13 (2) (2009) 124–148.

[3] W. Qin, S. Long, M. Panunzio, S. Biondi, Schiff Bbases: a short survey on an evergreen chemistry tool, Molecules 18 (10) (2013) 12264–12289.

[4] A.L. Berhanu, I.Mohiuddin Gaurav, A.K. Malik, J.S. Aulakh, V. Kumar, K.-H. Kim, A review of the applications of Schiff bases as optical chemical sensors, Trends Anal. Chem. 116 (2019) 74–91.

[5] K. Muller-Dethlefs, P. Hobza, Noncovalent interactions: a challenge for experiment and theory, Chem. Rev. 100 (1) (2000) 143–168.

[6] E.R. Johnson, S. Keinan, P. Mori-Sanchez, J. Contreras-Garcia, A.J. Cohen, W. Yang, Revealing noncovalent interactions, J. Am. Chem. Soc. 132 (18) (2010) 6498–6506.

[7] S. Gandhimathi, C. Balakrishnan, M. Theetharappan, M.A. Neelakantan, R. Venkataraman, Noncovalent interactions from electron density topology and solvent effects on spectral properties of Schiff bases, Spectrochim. Acta A 175 (2017) 134–144.

[8] C. Reichardt, T. Welton, Solvents and Solvent Effects in Organic Chemistry, 4th Ed, Wiley-VCH Verlag GmbH & Co. KGaA Weinheim, 2010.

[9] T. Rijavec, S. Bračko, 7 - Smart dyes for medical and other textiles, in: L. Van Langenhove (Ed.), Smart Textiles for Medicine and Healthcare, Woodhead Publishing, Oxford, 2007, pp. 123–149.

[10] A.A. Edwards, B.D. Alexander, UV-Visible absorption spectroscopy, organic applications, in: J.C. Lindon, G.E. Tranter, D.W. Koppenaal (Eds.), Encyclopedia of Spectroscopy and Spectrometry, 3rd Ed, Academic Press, Oxford, 2017, pp. 511–519.

[11] K.S.M. Salih, Y. Baqi, Microwave-assisted palladium-catalyzed cross-coupling reactions: generation of carbon–carbon bond, Catalysts 10 (1) (2020) 4.

[12] A.D. Becke, Density-functional exchange-energy approximation with correct asymptotic behavior, Phys. Rev. A 38 (6) (1988) 3098–3100.

[13] C. Lee, W. Yang, R.G. Parr, Development of the Colle-Salvetti correlation-energy formula into a functional of the electron density, Phys. Rev. B 37 (2) (1988) 785–789.

[14] I.Y. Zhang, J. Wu, X. Xu, Extending the reliability and applicability of B3LYP, Chem. Commun. 46 (18) (2010) 3057–3070.

[15] I. Badran, A. Rauk, Y. Shi, New orbital symmetry-allowed route for cycloreversion of silacyclobutane and its Methyl derivatives, J. Phys. Chem. A 123 (9) (2019) 1749–1757.

[16] I. Badran, A.D. Manasrah, Nashaat N. Nassar, A combined experimental and density functional theory study of metformin oxy-cracking for pharmaceutical wastewater treatment, RSC Adv 9 (24) (2019) 13403–13413.

[17] R. Ditchfield, W.J. Hehre, J.A. Pople, Self-Consistent molecular-orbital methods. IX. An extended gaussian-type basis for molecular-orbital studies of organic molecules, J. Chem. Phys. 54 (2) (1971) 724–728.

[18] J.B. Foresman, Æ. Frisch, Exploring Chemistry with Electronic Structure Methods, 3rd ed., Gaussian, Inc.: Wallingford, CT, USA2015.

[19] M.J. Frisch, G.W. Trucks, H.B. Schlegel, G.E. Scuseria, M.A. Robb, J.R. Cheeseman, G. Scalmani, V. Barone, B. Mennucci, G.A. Petersson, H. Nakatsuji, M. Caricato, X. Li, H.P. Hratchian, A.F. Izmaylov, J. Bloino, G. Zheng, J.L. Sonnenberg, M. Hada, M. Ehara, K. Toyota, R. Fukuda, J. Hasegawa, M. Ishida, T. Nakajima, Y. Honda, O. Kitao, H. Nakai, T. Vreven, J.A. Montgomery Jr., J.E. Peralta, F. Ogliaro, M. Bearpark, J.J. Heyd, E. Brothers, K.N. Kudin, V.N. Staroverov, R. Kobayashi, J. Normand, K. Raghavachari, A. Rendell, J.C. Burant, S.S. Iyengar, J. Tomasi, M. Cossi, N. Rega, J.M. Millam, M. Klene, J.E. Knox, J.B. Cross, V. Bakken, C. Adamo, J. Jaramillo, R. Gomperts, R.E. Stratmann, O. Yazyev, A.J. Austin, R. Cammi, C. Pomelli, J.W. Ochterski, R.L. Martin, K. Morokuma, V.G. Zakrzewski, G.A. Voth, P. Salvador, J.J. Dannenberg, S. Dapprich, A.D. Daniels, Ö. Farkas, J.B. Foresman, J.V. Ortiz, J. Cioslowski, D.J. Fox, Gaussian 09, Revision E.01, Gaussian Inc., Wallingford CT, 2009.

[20] N.M. O'boyle, A.L. Tenderholt, K.M. Langner, cclib: a library for package-independent computational chemistry algorithms, J. Comput. Chem. 29 (5) (2008) 839–845.

[21] K.S.M. Salih, A.M. Shraim, S.R. Al-Mhini, R.E. Al-Soufi, I. Warad, New tetradentate Schiff base Cu(II) complexes: synthesis, physicochemical, chromotropism, fluorescence, thermal, and selective catalytic oxidation, Emergent Mater 4 (2) (2021) 423–434.

[22] R.M. Silverstein, G.C. Bassler, T.C. Morrill, Spectrometric identification of organic compounds, 5th Ed, Wiley, New York, 1991.

[23] M. Makarska-Bialokoz, A.A. Kaczor, Computational analysis of Chlorophyll structure and UV-Vis spectra: a student research project on the spectroscopy of natural complexes, Spectroscopy Lett 47 (2) (2014) 147–152.

[24] J. Tomasi, B. Mennucci, E. Cancès, The IEF version of the PCM solvation method: an overview of a new method addressed to study molecular solutes at the QM ab initio level, J. Mol. Struct. THEOCHEM 464 (1) (1999) 211–226.

[25] D. Escudero, A.D. Laurent, D. Jacquemin, Time-dependent density functional theory: a tool to explore excited states, in: J. Leszczynski, A. Kaczmarek-Kedziera, T. Puzyn, M.G. Papadopoulos, H. Reis, M.K. Shukla (Eds.), Handbook of Computational Chemistry, Springer International Publishing, Cham, 2017, pp. 927–961.

[26] M.K. Hema, C.S. Karthik, N.K. Lokanath, P. Mallu, A. Zarrouk, K.S.M. Salih, I. Warad, Synthesis of novel Cubane [Ni4(O∩O)4(OCH3)4(OOH)4] cluster: XRD/HSA-interactions, spectral, DNA-binding, docking and subsequent thermolysis to NiO nanocrystals, J. Mol. Liq. (2020) 315.

[27] A. Guerraoui, A. Djedouani, E. Jeanneau, A. Boumaza, A. Alsalme, A. Zarrouk, K.S.M. Salih, I. Warad, Crystal structure and spectral of new hydrazine-pyran–dione derivative: DFT enol↔hydrazone tautomerization via zwitterionic intermediate, hirshfeld analysis and optical activity studies, J. Mol. Struct. 1220 (2020).

[28] N. Al-Zaqri, K.S.M. Salih, F.F. Awwadi, A. Alsalme, F.A. Alharthi, A. Alsyahi, A.A. Ali, A. Zarrouk, M. Aljohani, A. Chetouni, I. Warad, Synthesis, physicochemical, thermal, and XRD/HSA interactions of mixed [Cu(Bipy)(Dipn)](X)2 complexes: DNA binding and molecular docking evaluation, J. Coord. Chem. 73 (23) (2020) 3236–3248.

[29] A. Boshaala, K.S.M. Salih, N. Bader, A.A. Almughery, A. Zarrouk, I. Warad, XRD/HSA, noncovalent interactions and influence of solvent polarity on spectral properties of dithiocarbazate schiff base and its cis-Cu(II) complex: Experimental and theoretical studies, J. Mol. Liq. 330 (2021) 115551.

[30] E.S. Dodsworth, M. Hasegawa, M. Bridge, W. Linert, in: 2.27 - Solvatochromism Comprehensive Coordination Chemistry II, Pergamon, Oxford, UK, 2003, pp. 351–365.

[31] U. Mayer, V. Gutmann, W. Gerger, The acceptor number ? A quantitative empirical parameter for the electrophilic properties of solvents, Monatsh. Chem. 106 (6) (1975) 1235–1257.

[32] C. Franco, A revision of the Gutmann donor numbers of a series of phosphoramides including TEPA, Eur. Chem. Bull. 4 (2015) 92–97.

[33] J. Tauc, R. Grigorovici, A. Vancu, Optical properties and electronic structure of amorphous germanium, Phys. Status Solidi B 15 (2) (1966) 627–637.

[34] A. Dolgonos, T.O. Mason, K.R. Poeppelmeier, Direct optical band gap measurement in polycrystalline semiconductors: a critical look at the Tauc method, J. Solid State Chem. 240 (2016) 43–48.

[35] P. Makuła, M. Pacia, W. Macyk, How to correctly determine the band gap energy of modified semiconductor photocatalysts based on UV–Vis spectra, J. Phys. Chem. Lett. 9 (23) (2018) 6814–6817.

[36] N. Soltani, E. Saion, M.Z. Hussein, M. Erfani, A. Abedini, G. Bahmanrokh, M. Navasery, P. Vaziri, Visible light-induced degradation of methylene blue in the presence of photocatalytic ZnS and CdS nanoparticles, Int. J. Mol. Sci. 13 (10) (2012) 12242–12258.

[37] A.G. Pramod, Y.F. Nadaf, C.G. Renuka, A combined experimental theoretical approach for energy gap determination, photophysical, photostable, optoelectronic, NLO, and organic light emitting diode (OLED) application: Synthesized coumarin derivative, J. Mol. Struct. 1194 (2019) 271–283.

[38] M.R. Alam, G. Alwarappan, A. Bhandari, S. Patil, S. Alfalah, M.F. Shibl, W.M.I. Hassan, R. Nekovei, A. Verma, TDDFT studies on sheet size-dependency of optoelectronic properties of 2D silicon, in: 2018 IEEE 13th Nanotechnology Materials and Devices Conference (NMDC), 2018, pp. 1–4.

[39] J.-L. Bredas, Mind the gap!, Mater. Horiz. 1 (1) (2014) 17–19.

[40] A. Yoshikawa, H. Matsunami, Y. Nanishi, Development and applications of wide bandgap semiconductors, in: K. Takahashi, A. Yoshikawa, A. Sandhu (Eds.), Wide Bandgap Semiconductors: Fundamental Properties and Modern Photonic and Electronic Devices, Springer Berlin Heidelberg, Berlin, Heidelberg, 2007, pp. 1–24.